DOE-ER-40427-01-N92

Fermilab Library
0 1160 0007115 3

34

DOE-ER-40427-01-N92

Nucleon Models of Deep Inelastic Scattering

Gerald A. Miller

Department of Physics, FM-15

University of Washington, Seattle, Washington 98195

ROUTE TO
LOCATION
RETURN TO FERMI LIBRARY

Proceedings, RIKEN Winter Seminar

"Quarks and Gluons in Nucleons and Nuclei"

Yuzawa, Japan, January 1992

PREPARED FOR THE U.S. DEPARTMENT OF ENERGY

This report was prepared as an account of work sponsored by the United States Government. Neither the United States nor the United States Department of Energy, nor any of their employees, nor any of their contractors, subcontractors, or their employees, makes any warranty, express or implied, or assumes any legal liability or responsibility for the product or process disclosed, or represents that its use would not infringe privately-owned rights.

By acceptance of this article, the publisher and/or recipient acknowledges the U.S. Government's right to retain a nonexclusive, royalty-free license in and to any copyright covering this paper.

Nucleon Models of Deep Inelastic Scattering

Gerald A. Miller

University of Washington, Department of Physics, FM-15
Seattle, Washington, 98195

Abstract

Nucleon models should describe both deep inelastic scattering and low energy phenomenology. We review some recent calculations of valence quark distributions. Models in which the valence quarks are the only dynamical variables fail to describe the data, since the valence quarks saturate the energy-momentum sum rule. This is in sharp disagreement with existing data[1] which indicate that a substantial fraction of the nucleon's momentum is carried by glue and sea even for Q^2 as low as 0.5 GeV^2.

1. Introduction

Quantum chromodynamics QCD is the present candidate for the true theory of the strong interaction. This is a theory of quarks and gluons. Thus it is very important to understand lepton-nucleon deep inelastic scattering. The approximate scaling properties of such data provided striking evidence for the existence of quarks[2]. Furthermore, the small deviations from scaling provide evidence for the existence of gluons[2].

It is well known that the techniques of perturbation QCD can be used to relate quark distribution functions $q(x, Q_1^2)$ and $q(x, Q_2^2)$ measured at different values of four momentum transfer squared. However nonperturbative techniques are necessary to obtain one of the $q(x, Q_i^2)$. The physics of confinement and dynamical symmetry breaking must be applied.

Lattice gauge theory is regarded as the favorite technique for non-perturbative calculations. However, such calculations have not been widely applied to computing $q(x, Q^2)$.

Instead we shall discuss models of confinement. Such models are based on a guess about the true nature of QCD. For example, the MIT bag model[3] is built on the premise that quarks are essentially free from interaction over the entire volume of the nucleon. The cloudy bag model[4] improves upon this by the incorporation of pion cloud effects. The soliton bag model[5,6,7] treats the surface as a dynamical variable. The skyrmion model[8] treats the nucleon as a non-topological soliton built from meson fields.

Such models are often applied to low energy phenomena. Our view is that a model is incomplete unless it can be applied to the computation of $q(x, Q^2)$. This provides a severe test. Some models will surely fail. We shall argue that models in which quarks are the only dynamical values are doomed to failure in describing deep inelastic scattering.

Another motivation for obtaining an improved understanding of quark distribution functions is the EMC effect.[9] Since 1982 much effort has been made to understand

the effects of the nuclear medium on the quark distributions of individual nucleons. One must understand the true nature of the quark distribution before asking how or if medium effects change that distribution.

Our purpose here is to review the very excellent thesis work of Charles Benesh[10-13]. The necessary background formalism[14,15] is discussed in Sect. 2. The MIT bag model is applied in Sect. 3. A cloudy bag model which incorporates the important effects of surface dynamics is reviewed and applied in Sect. 4. The soliton bag model provides a qualitatively accurate representation of the valence quark distribution functions, as explained in Sect. 5. A final section is reserved for summary remarks.

2. Quark Distribution Functions Measured by Deep Inelastic Scattering

Start with the photon quark interaction. The current $J_\nu(\xi)$ is given by

$$J_\nu(\xi) = \bar{\psi}(\xi)\gamma_\nu\, q\, \psi(\xi) \tag{1}$$

Where $\psi, \bar{\psi}$ are quark field operators and Q is the diagonal quark charge matrix with elements $e(2/3, -1/3, -1/3)$. The DIS reaction is depicted in Fig. 1. A photon of four-momentum q is absorbed on a quark from the target of momentum P. The final state X, has momentum P_X.

The differential cross section $d\sigma$ is proportional to the contraction of the lepton tensor $\ell_{\mu\nu}$ with the interesting nuclear (or nucleon) matrix element $W^{\mu\nu}$,

$$d\sigma \propto \ell_{\mu\nu} W^{\mu\nu} \tag{2}$$

with

$$W^{\mu\nu} \propto \sum_X \int d^4x d^4y \langle P|J^\mu(x)|P_X\rangle\langle P_X|J^\nu(y)|P\rangle \delta^{(4)}(P+q-P_X). \tag{3}$$

Equation (3) is obtained from Fermi's golden rule. One sums over all final states X that are consistent with conservation of energy and momentum.

Hence the four-dimensional delta function appears. One may use translational invariance, completeness, and the subtraction of a vanishing term to arrive at the result

$$W^{\mu\nu} = \frac{1}{4\pi}\int d^4\xi e^{iq\cdot\xi} < P|\,[J^\mu(\xi), J^\nu(0)]\,|P >_c . \tag{4}$$

The subscript c denotes the necessity of including only connected matrix elements.

In an exclusive (e, e') or (μ, μ') scattering experiment one measures the energy and scattering angle of the outgoing lepton (e' or μ'). Thus there are two variables. The preferred choice for high energy DIS is to use

$$Q^2 = -q_\mu q^\mu \tag{5}$$

(Q^2 is positive for DIS) and, x with

$$x = Q^2/(2P\cdot q). \tag{6}$$

The photon energy q^0 is written as $\nu(\nu = q^0)$ so that in the rest frame of the target $(P^0 = M)$

$$x = Q^2/(2M\nu). \tag{7}$$

Thus $W^{\mu\nu}$ is a function of the two variables $W^{\mu\nu}(x, Q^2)$.

The direction of the z-axis is chosen to be antiparallel to the photon's momentum so that

$$q^\mu = (\nu, 0, 0, -q^3). \tag{8}$$

The Bjorken limit of $Q^2, \nu)$ going to infinity with x held fixed is very useful. In this kinematic regime scaling arises simply from the condition that the photon-quark absorption obeys conservaton of energy and momentum. The essential assumption is that a quark of four momentum xP absorbs the photon of momentum q. One finds $(xP+q)^2 = mq^2 = (xP)^2$. Thus $x = Q^2/2P\cdot q$. If the nucleon momentum is very large

(as in the infinite momentum frame) xP stands for both the energy and momentum of the quark. Components of the quark momentum that are perpendicular to the direction of the infinite momentum are ignorable. In the target rest frame xP stands for the sum of the quark's energy and z-momentum. We shall use the target rest frame, since the models we use are defined in that frame. One may remove q^3 from Eq. (8) by using $Q^2 = (q^3)^2 - \nu^2$ and the Bjorken limit. Then one finds

$$q^\mu = (\nu, 0, 0, -\nu - Mx), \tag{9}$$

which suggests a new set of variables

$$q^\pm = \frac{1}{\sqrt{2}}(q^0 \pm q^3) \tag{10}$$

with $\vec{q}_\perp = q_1\hat{i} + q_2\hat{j} = 0$. The definition (10) is nice because, with (9) and the Bjorken limit q^+ is finite and q^- is not:

$$q^+ = \frac{1}{\sqrt{2}}(Mx) \tag{11}$$

$$q^- = -\sqrt{2}\nu. \tag{12}$$

The four vector dot product $q \cdot \xi$ appearing in Eq. (4) is then

$$q \cdot \xi = q^+\xi^- + q^-\xi^+. \tag{13}$$

The infinite nature of q^- in the Bjorken limit simplifies the integral appearing in Eq. (4). The term $J_\mu(\xi)$ is evaluated at $\xi^+ = 0$, otherwise the rapid variation of the phase causes the integral on $d\xi^+$ to vanish. Indeed, there can only be a contribution if the current commutator has a singularity at $\xi^2 = 0$.

In the present notation (Eqs. 8-12) the structure function F_2 is given by

$$F_2(x) = 2xW_{11} = \frac{x}{2\pi}\int d^4\xi e^{iq\cdot\xi} < P|\,[J_1(\xi), J_1(0)]\,|P >_c . \tag{14}$$

The quantity $F_2(x)$ is proportional to the imaginary part of the Feynman diagram of Fig. 2, with the intermediate high momentum quark acting (briefly) as a free fermion. The most singular (most important) term of the free quark propagator S_F is given in the Bjorken limit as

$$S_F = i\gamma^+ q^- \frac{1}{2\pi}\delta(\xi^2)\,\epsilon(\xi^0). \tag{15}$$

The factor $\gamma^+ q^-$ is the non-zero remainder of the typical $\not{q}$ term appearing in the rationalized Feynman propagator. The γ^+ appears early and remains to the end of the presentation. The $\delta(\xi^2)$ indicates that the effectively massless ($Q^2 \to \infty$) quarks propagate with the speed of light. The factor $\epsilon(\xi^0)$ is[5] +1 if $\xi^0 > 0$ and -1 if $\xi^0 < 0$.

The evaluation of Eq. (14) using Eq.(2) and the propagator S_F (Eq. 15) leads to[3]

$$F_2(x) = \frac{x}{4\pi}\int d\xi^- e^{iq^+\xi^-} < P|\bar{\psi}(\xi^-)\gamma^+ Q^2\psi(0)$$

$$-\bar{\psi}(0)\gamma^+ Q^2\psi(\xi^-)|p >_x \Big|_{\xi^+=\vec{\xi}_\perp=0} \tag{16}$$

where [recall Eq. (11)] $q^+ = -\frac{1}{\sqrt{2}}Mx$.

One may rewrite (16) in terms of quark (antiquark) distribution functions $q_A(x), (q_a(x))$:

$$F_2(x) = x\sum_a (q_a(x) + q_{\bar{a}}(x))Q_a^2 . \tag{17}$$

Here $q_a(x)$ arises from the $\bar{\psi}(\xi^-)\gamma^+ Q^2\psi(0)$ term of Eq. (16). The relations between $q_a(x_A)$ and $q_a(x)$ and the matrix elements of Eq. (16) are discussed in Ref. (14). Basically $q_a(x)$ is the probability that a quark of flavor a carries a momentum fraction x. If the quark has plus-momentum $k^+, x = k^+/P^+$.

3. Deep-inelastic Structure Functions in the MIT Bag Model[10,11]

We discuss progress toward the calculation of quark distributions in the MIT bag model. Previous calculations of this type suffer either from the lack of translational

invariance of the bag wave functions[16], or from the assumptions necessary to ensure momentum conservation. Here we use a Peierls-Yoccoz-projected MIT bag wave function for the nucleon and calculate the Bjorken limit of the current-current correlation function. These distributions are interpreted as the twist-two piece of the nucleon structure function evaluated at a low-momentum scale $Q^2 = \mu_0^2 \simeq 0.5$ GeV^2. QCD perturbation theory is then used to evolve the distributions to $Q^2 = 15$ GeV^2, where higher-twist effects are small, and comparison with experiment is made.

In the calculations that follow, we shall adopt a point of view suggested by Jaffe and Ross.[15] In particular, we shall assume that the calculations of structure functions in the bag represent the twist-two piece of the physical structure function evaluated at a low value of $Q^2 = \mu_0^2$. The motivation for this is the observation from QCD that the quark structure of the nucleon changes with the scale Q^2 at which one probes it. Thus, if the nucleon looks like three valence quarks in a confining interaction at some scale μ_0^2, radiative QCD corrections will change is composition at higher Q^2. Quarks will radiate gluons and these in turn will pair produce quarks until the nucleon becomes a very complicated object.

Knowing the twist-two piece of the structure function at $Q^2 = \mu_0^2$, we may then use QCD perturbation theory to evolve to high Q^2. At high enough Q^2, higher-twist effects become negligible and we may compare the resulting distribution functions with data. Note that this prescription implies that the structure functions calculated at $Q^2 = \mu_0^2$ should not look like *any* data, since the physical structure function will certainly have important contributions from all twists at this scale.

Finally, we need to decide upon a reasonable value for μ_0^2. Jaffe and Ross determine μ_0^2 by performing a fit of the ratios of evolved and unevolved moments to the predictions of second-order QCD. Here, we will simply require that μ_0^2 be a scale characteristic of a single nucleon. In the bag model, there is only one scale, the bag radius. Hence, we shall

take $\mu_0^2 \simeq 1/R^2 \sim 0.5$ GeV^2. Since QCD evolution depends on μ_0^2 only logarithmically, the precise value of μ_0^2 is not critical to our results. Indeed, we shall see later that varying μ_0^2 by 20% produces little change in our quark distributions.

In order to proceed further, we must specify the nucleon wave function $|P\rangle$ of Eqs. (16) and (17). We choose a Peierls-Yoccoz-projected version of the usual MIT bag ground state:

$$|N, \mathbf{P} = 0\rangle = \lambda \int d^3a |\mathbf{R} = \mathbf{a}\rangle \ , \tag{18}$$

where

$$|\mathbf{R} = \mathbf{a}\rangle \equiv b_0^\dagger(\mathbf{a}) b_0^\dagger(\mathbf{a}) b_0^\dagger(\mathbf{a}) |EB; \mathbf{R} = \mathbf{a}\rangle \tag{19}$$

is an unprojected MIT bag state centered at $\mathbf{R} = \mathbf{a}$, $b_0^\dagger(\mathbf{a})$ is the creation operator for the lowest quark mode, and $|EB; \mathbf{R} = \mathbf{a}\rangle$ is an empty bag state centered at $\mathbf{R} = \mathbf{a}$. (Flavor-spin and color indices are not made explicit.) The factor λ is chosen so that the state $|N, \mathbf{P} = 0\rangle$ satisfies the covariant normalization for momentum eigenstates.

The advantage of this state is that it is an exact eigenstate of momentum. Thus, problems related to translational invariance will not arise. Potential problems are the fact that $|N\mathbf{P} = 0\rangle$ is not an exact eigenstate of energy, and determining the mass that appears in the expression for λ. These issues are addressed in Refs. 10 and 11.

To obtain the mass M, we perform a variational calculation of

$$\langle H_{MIT}\rangle = \frac{\langle N, \mathbf{P} = 0 | H_{MIT} | N, \mathbf{P} = 0\rangle}{\langle N, \mathbf{P} = 0 | N, \mathbf{P} = 0\rangle} \ . \tag{20}$$

Minimizing $\langle H_{MIT}\rangle$ with respect to the bag radius R, we obtain an approximate solution for the ground state and mass. The details are given in Ref. 10.

We confine our attention to the valence distribution $q_v(x) = q(x) - \bar{q}(x)$. By computation, this distribution is seen to satisfy the normalization and momentum constraints to a reasonable approximation. The resulting[10] valence distribution is shown in Fig. 3 along with the analogous unprojected result.

3.1 QCD Evolution

The valence-quark distributions calculated in the previous section are evolved from $Q^2 = \mu_0^2 = 0.5$ GeV^2 to $Q^2 = 15$ GeV^2 using second-order QCD perturbation theory, with[17] $\Lambda_{QCD} = 150$ MeV. One may ask whether or not perturbation theory may be trusted at such low values of Q^2. Pennington and Ross[18] have argued that not all QCD perturbation expansions need be equally convergent and certain "good" predictions may be obtained, independent of the renormalization scheme, which appear to converge very fast. The nonsinglet evolution equations are an example of such "good" predictions and we hope that it will reliably interpolate between the bag scale μ_0^2 and experiment at high Q^2.

The results of the evolution are shown in Fig. 4 for first ($\mu_0^2 = 0.5$ GeV^2) and second ($\mu_0^2 = 0.4, 0.5, 0.6$ GeV^2) order; also shown are data from the CERN-Dortmund-Heidelberg-Saclay (CDHS) Collaboration.[1] The relative smallness ($\sim 10\%$) of the second-order QCD corrections give some credence to the idea that perturbation theory is applicable at the bag scale. One should also note the slow variation of our results with changing μ_0^2.

3.2 MIT Bag Model

We begin this section by reviewing the consistency of our calculations. First, note that the valence quarks are the only objects in the bag that carry momentum, so the valence quarks should carry all the momentum. This means that

$$N \equiv \int_0^1 dx\, q_v(x) = 1 \quad \text{and} \quad \langle x \rangle \equiv \int_0^1 dx\, x q_v(x) = \frac{1}{3}$$

at the bag scale.

Numerically, we find $N \simeq 1.004$ and $\langle x \rangle \simeq 0.312$. Thus, roughly 6% of the bag's momentum is "missing" in our calculation. There are several possible explanations for this.[10] It seems that our approximations are reasonable to within about 6%.

In Fig. 3 we see that the projected calculation has vastly improved support properties when compared with the unprojected result. At $x = 1$, the projected quark distributions are 30 times smaller than the unprojected ones and are decreasing more rapidly. Thus, admixtures of mass states other than the ground state are quite small.

Comparison of the evolved valence distributions with experimental data gives no agreement at all. The calculated values of $xq_v(x)$ are roughly a factor of 2 larger than experiment. This may have been anticipated before any calculations were made. To see this, consider the following argument:[27] In *any* model that contains only valence quarks, those quarks must carry all the momentum in the bag. If we associate the scale $\mu_0^2 \simeq 0.5$ GeV^2 with this model, then evolution to 10 GeV^2 gives valence-quark distributions that carry momentum fraction

$$\langle x \rangle = \frac{1}{3}\left[\frac{\ln \mu_0^2/\Lambda_{QCD}^2}{\ln Q^2/\Lambda_{QCD}^2}\right]^{0.395} = 0.255$$

with $\Lambda_{QCD} = 150$ MeV.

Experimentally[19], one finds $\langle x \rangle = 0.155$ for μ quarks, and $\langle x \rangle = 0.12$ for d quarks. Since $\langle x \rangle$ is simply the area under the curve $xq_v(x)$, we see that *any* quark-model calculation will yield valence distributions roughly twice as large as experiment.

A simple solution to this difficulty[20] is to choose a different value for μ_0^2 such that $\langle x \rangle$ agrees with experiment at high Q^2. Using second-order QCD, we determine this value of μ_0^2 to be around 0.1 GeV^2. In terms of distances, this corresponds to about 2.2 R_N. This distance scale seems too large to be associated with the physics of a single nucleon. Furthermore, the perturbative analysis for the moments is not trustworthy at this scale.

A more realistic possibility, we feel, is to keep $\mu_0^2 \simeq 0.5$ GeV^2 and to add new components to the nucleon wave function. These new dynamical variables carry momentum, and the right combination may be found to reproduce the data. Among the possibilities

for these new degrees of freedom are pions, sea quarks, collective oscillations of the bag surface, and explicit gluons in the bag wave function.

The quark distributions we have calculated have, to a very good approximation, the support properties required by energy-momentum conservation. Thus, they provide a foundation for further calculations of quark distributions in nucleons and, once that is complete, nuclei.

4. Deep-inelastic Scattering in a Vibrating Bag Model[10,12]

In the previous calculation[3], we obtained valence-quark distributions for a Peierls-Yoccoz momentum-projected version of the MIT bag. Those distributions have the correct support properties as a function of the Bjorken scaling variable x, but the valence quarks saturate the energy-momentum sum rule, in sharp disagreement with existing data[1] which indicate a substantial fraction of the nucleon's momentum is carried by glue and sea, even at low-momentum transfers $Q^2 \simeq 0.5$ GeV^2. This problem is shared by all models in which the valence quarks are the only dynamical objects, and clearly indicates a need for more complete models.

We next discuss our investigation of one such model. Specifically, we consider a bag model with a kinetic-energy term for the bag radius $R(t)$, thus transforming $R(t)$ into a dynamical variable. Our interpretation is that $R(t)$ represents the nonperturbative gluonic degrees of freedom responsible for confining the valence quarks. As in Refs. 10, 11 we will use Peierls-Yoccoz projection to obtain an eigenstate of zero momentum, and then calculate the Bjorken limit of the current-current correlation function. These distributions are interpreted as the twist two piece of the nucleon structure function evaluated at a low-momentum scale $Q^2 = \mu_0^2 \simeq 0.5$ Gev^2. QCD perturbation theory is then used to evolve these distributions to $Q^2 = 15$ GeV^2, where higher-twist effects are small, and comparison with experiment is made.

4.1 The Model

The model we shall use was originally formulated by Dirac[21] as a theory of the electron, and later applied to hadronic physics by the Budapest group.[22] Although we shall consider only spherically symmetric bags, this model contains all possible excitations of the surface and is derived from a Lorentz-scalar Lagrangian.

Before describing any further details of the model, it is convenient to present the formalism for the adiabatic approximation used to solve it. Begin by defining the Peierls-Yoccoz projected momentum state of radius R:

$$|\mathbf{p}=0;R\rangle = \lambda(R)\int d^3a\; b_0^\dagger(\mathbf{a})b_0^\dagger(\mathbf{a})b_0^\dagger(\mathbf{a})|EB;R,\mathbf{a}\rangle = \int d^3a|R,\mathbf{a}\rangle\ . \tag{21}$$

Here $|EB;\mathbf{R}\rangle$ is an empty bag state of radius R centered at $\mathbf{a}$, $b_0^\dagger(\mathbf{a})$ acting on $|EB;R\mathbf{a}\rangle$ creates a quark in the lowest cavity model of a bag of radius R (color and flavor indices have been suppressed), and $\lambda(R)$ is chosen so that the state $|\mathbf{p}=0,R\rangle$ satisfies the covariant normalization for momentum eigenstates

$$\lambda^2(R) \equiv \frac{2M}{\int d^3a\langle 0,R|R,a\rangle}\ , \tag{22}$$

where M is the physical mass of the system.

In the adiabatic approximation, one assumes that energy eigenstates are given by

$$|N\mathbf{p}=0\rangle = \int_0^\infty dR\;\phi(R)|\mathbf{p}=0;R\rangle\ , \tag{23}$$

where $\phi(R)$ is a probability amplitude for finding a bag of radius R.

Furthermore, one typically assumes that[12]

$$\langle\mathbf{p}=0;R|\mathbf{p}=0;R'\rangle = \delta(R-R')2M\delta^3(0)(2\pi)^3\ , \tag{24}$$

so that the normalization condition becomes

$$\int_0^\infty dR\;\phi^2(R) = 1\ . \tag{25}$$

The remaining ingredient required is a method for determining $\phi(R)$, which we now provide. Begin by writing down the action for a free relativistic membrane:

$$S = \frac{-\mu^3}{4\pi} \int dt \int dA (1 - V_T^2)^{1/2} , \tag{26}$$

where $\mu^3/4\pi$ is the surface tension and $\mathbf{V}_T$ is the velocity of a surface point transverse to the surface.

This action is proportional to the volume of the hypertube swept out by the surface in Minkowski space, and is consequently Lorentz invariant. Restricting our attention to spherical surfaces, the action becomes

$$S = -\mu^3 \int dt\, R^2 (1 - \dot{R}^2)^{1/2} \tag{27}$$

from which we may easily derive the conjugate momentum P_R and the surface Hamiltonian H_S:

$$P_R = \frac{\delta L}{\delta \dot{R}} = \frac{\mu^3 R^2 \dot{R}}{(1 - \dot{R}^2)^{1/2}} ,$$
$$H_S = P_R \dot{R} - L = \frac{\mu^3 R^2}{(1 - \dot{R}^2)^{1/2}} = [(\mu^3 R^2)^2 + P_R^2]^{1/2} . \tag{28}$$

Quantize the surface motion ($P_R \leftrightarrow -i d/dR$) to obtain

$$H_S = \left[\frac{-d^2}{dR^2} + (\mu^3 R^2)^2 \right]^{1/2} . \tag{29}$$

Now add the quarks to obtain the full adiabatic Hamiltonian

$$H = H_S + H_{MIT}(R) + H_{OGE}(R) + H_{ZP}(R) + H_{OPE}(R) , \tag{30}$$

where each of the terms is explained below.

Now we exlain the remaining terms of the Hamiltonian (30). The first term is the usual MIT bag Hamiltonian:

$$H_{MIT} = \frac{3\varepsilon}{R} + \frac{4\pi}{3} B R^3 , \tag{31}$$

where $\varepsilon = 2.04$.

The next term H_{OGE} is the one-gluon-exchange contribution to the quark energy. We evaluate this energy using the original calculation of Degrand *et al.*[3] except that we allow the strong coupling constant to vary with the bag radius in a manner consistent with asymptotic freedom:

$$\alpha_s(R) = \frac{\alpha_0}{\left\{ 1 + [\ln(1/\Lambda R)]^2 \right\}^{1/2}} \equiv \alpha_0(R) \tag{32}$$

with $\Lambda = 150$ MeV. For large radii, $\alpha_s(R)$ tends to vanish, contrary to the usual QCD picture. This is not a problem, however, as the volume and surface contributions to the Hamiltonian cause the wave function to be small in this region ($R \gg 1$ fm). Thus, collecting numerical factors, we have

$$H_{OGE}(R) = -3\lambda_T \beta \frac{g(R)}{R} , \tag{33}$$

where β is a numerical factor and $\lambda_T = +1, -1$ for spin-$\frac{1}{2}$ and spin-$\frac{3}{2}$ eigenstates, respectively.

The third term in (30) represents the contribution to the energy of the zero-point fluctuations of the quark and gluon fields. For this, we shall use an expression due to Johnson:[23]

$$H_{ZP} = \frac{8a_G}{R} + \frac{9a_Q}{R} - \frac{b\alpha_s(R)}{R} , \tag{34}$$

where $a_G = 0.04618$ is an exact result from QED, a_Q represents the zero-point energies of three flavors of quarks, and the last term is a contribution from the self-interactions of the gluons. Naively, we expect $a_Q = 2a_G$ since there are twice as many fermion polarizations as gluon polarizations. However, the spectrum of gluons is different from that of the fermions due to different boundary conditions, so that the actual value of a_Q does not equal $2a_G$, and depends on the geometry involved. For two parallel plates[3],

$a_Q = \frac{7}{4} a_G$. We shall take this as a representative value for a_Q/a_G. Thus, we have

$$H_{ZP} = \frac{1.097}{R} - \frac{Zg(R)}{R} , \tag{35}$$

where Z remains a parameter to be determined.

The last term in (30) is the coupling of pions to the bag. We use the volume coupled version[4] of the cloudy bag and treat pionic effects perturbatively. The formalism for calculating one-pion-exchange effects is identical to the usual cloudy bag formalism, except that the usual form factor, given by $3j_1(KR)/KR$, where K is the momentum of the emitted pion, is replaced by

$$F_{ij}(K) = \int dR\, \phi_i^*(R) \frac{3j_1(KR)}{KR} \phi_j(R) , \tag{36}$$

where ϕ_i and ϕ_j are the collective wave functions of the initial and final states.[24]

Before proceeding further, it is worthwhile to point out that the procedure outlined above amounts to a variational of the mass *before* projecting onto a state of good momentum. This has two practical consequences. First, it means that the wave function we obtain will contain not only the ground state, but admixtures of higher excited states as well. This follows simply from the fact that the variational calculation is not exact. The second consequence is that the energies we obtain contain contributions from spurious center-of-mass motion and consequently are too large. We correct for this by subtracting

$$M = E - \frac{\langle P^2 \rangle}{2E}$$
$$P^2 = P_q^2 + P_R^2 , \tag{37}$$

where E is the variationally determined energy, $\mathbf{P}_q$ is the quark momentum operator, and P_R is the surface momentum from (28).

4.2 Low-Energy Phenomenology

As described, the model contains four parameters, the bag constant B, the surface tension μ, the strong coupling constant β, and the zero-point parameter Z. By requiring a reasonable fit (10-15%) to the nucleon, Roper, and Δ masses, and to the nucleon charge radius, we determine the parameters to be

$$B^{1/4} = 117 \text{ MeV}, \quad \mu = 195 \text{ MeV} ,$$
$$\beta = 0.75, \quad Z = 2.35 . \tag{38}$$

The data used for the fit are summarized in Table I. The masses are listed before ("bare") and after ("dressed") applying lowest-order pionic corrections.

Table I. Low-energy scattering data and masses

Quantity	Bare	Dressed (one pion)	Experiment
M_N(MeV)	1200	1097	940
M_Δ(MeV)	1477	1370	1230
M_R(MeV)	1560	1433	1440-1470
$\langle r_{ch}^2 \rangle_N^{1/2}$(fm)	0.91		0.83
μ(fm)	0.24		0.29

The model is in reasonable agreement with the low energy data, so we turn to high-energy properties.

4.3 Deep-inelastic Scattering

The valence-quark distributions of the nucleon are obtained from a two-step procedure. First, we calculate quark distributions for the bare nucleon and several bare resonances using the methods deveooped in Ref. 3. The second step is to include one-pion-exchange effects using the convolution formalism of Sullivan.[25] We interpret the

result as the twist two piece of the physical structure function evaluated at a low-momentum scale $Q^2 \equiv \mu_0^2 \simeq 0.5$ GeV^2. QCD perturbation theory is then used to evolve the distribution to $Q^2 = 15$ GeV^2, where it is compared with experiment. We also include one-pion-exchange effects using the convolution formulas commonly seen in discussions of the EMC effect.[26] Instead of calculating $F_2(x)$, we write instead the contributions to individual valence-quark distribution following the work of Nikolaev.[27] See also Ref. 10.

The result of the full calculation is the valence-quark distribution $u_v(x) - d_v(x)$ shown in Fig. 5 along with the MIT bag distribution from Refs. 10,11. The additional spreading of the quark distribution is due to the spread in the quark's momentum-space wave function caused by the surface motion. The corresponding reduction in peak height is necessary in order to satisfy the Callan-Gross sum rule. The main effect of the pion coupling is the rescaling of x due to the nucleon mass shift. The distribution has a sizable tail at $x \simeq 1$, indicating that the variational procedure has not been a complete success and that there is an admixture of higher-mass states in our wave function. Thus, the distribution shown in Fig. 5 is a superposition of the quark distributions of several particles and there is considerable uncertainty associated with the quark distribution, especially at large x. A lower bound on this uncertainty is the ratio of the tail height to the peak height ($\simeq$ 10%). An upper bound of about 30% may be estimated by comparing the tail heights of the bare nucleon and Roper resonances. In any case, we expect the shape and size of the distribution to be more reliable at low and intermediate x.

4.4 Summary of modified bag model results

The first conclusion we draw is that bag dynamics play a large role in determining the deep-inelastic structure of the nucleon.

Taken together, our calculations of low- and high-energy observables seem to indicate that the model provides an adequate description of the nucleon. This conclusion is obscured by the uncertainties associated with the adiabatic approximation, and the Peierls-Yoccoz procedure used to eliminate center-of-mass problems. It would be advantageous to consider these questions in a model where they may be addressed more directly, such as the soliton bag.

5. Valence Quark Distributions in the Soliton Bag Model[12]

In the simplest version of the soliton bag model confinement is provided by a dynamical scalar field σ. The calculations to follow are performed using the coherent state projection techniques developed by Wilets et al. [5] and the Friedberg-Lee [6] soliton model. The lagrangian for the model is given by

$$\mathcal{L} = i\bar{\psi}\gamma_\mu\partial^\mu\psi - g\sigma\bar{\psi}\psi + \tfrac{1}{2}(\partial_\mu\sigma)^2 - U(\sigma), \tag{39}$$

where $U(\sigma) = \frac{1}{2}a\sigma^2 + (b/3!)\sigma^3 + (c/4!)\sigma^4 + d\sigma + p$.

In ref. [5], the model is solved by making a trial wavefunction for the ground state of the form

$$|n\rangle = \int d^3 b^+(\vec{a}) a\, b^\dagger(\mathbf{a}) b^\dagger(\mathbf{a}) |EB; \mathbf{a}\rangle, \tag{40}$$

where the $b^\dagger$'s create quarks whose wavefunctions are $\psi_0(\mathbf{r} - \mathbf{a})$ and

Table 2. Low-energy nucleon properties

Low energy observables	Calculated	Experiment[a)]
E_N	930 MeV	939 MeV
ϵ_q	279 MeV	
ϵ_{OGE}	-100 MeV	
ϵ_σ	193 MeV	
$\langle r_N^2 \rangle^{1/2}$	0.83 fm	0.83 fm
μ_p	2.67	2.76
g_A	1.27	1.26

[a)] From ref. [5].

$$|EB;\mathbf{a}\rangle = \exp\left(\int d^3k\sqrt{\tfrac{1}{2}\omega_k}e^{i\mathbf{k}\cdot\mathbf{a}}f(\mathbf{k})a_k^\dagger\right)|0\rangle \tag{41}$$

is a coherent state of the σ field with mean value $\sigma_0(\mathbf{r}-\mathbf{a})$. The functional forms of ψ_0 and σ_0 are given by

$$\begin{aligned}\sigma_0(\mathbf{r}) - \sigma_v &= [\tilde{\sigma}_0(\mathbf{r}/\lambda) - \sigma_v],\\ \psi_0(\mathbf{r}) &= \begin{pmatrix}\tilde{U}(r/\lambda)\\ i\sigma\cdot\hat{\mathbf{r}}\gamma\tilde{V}(r/\lambda)\end{pmatrix},\end{aligned} \tag{42}$$

where the functions $\tilde{\sigma}, \tilde{U}$ and $\tilde{V}(r)$ are the mean field solutions of the model, and γ and λ are variational parameters.

The state described in Eq. (36) is manifestly an eigenstate of zero momentum. An approximate energy eigenstate is obtained by minimizing the hamiltonian derived from (35)

$$\langle H\rangle = \frac{\langle N|H|N\rangle}{\langle N|N\rangle} \tag{43}$$

and identifying $\langle H\rangle$ as the ground state mass.

Using these methods, Wilets et al. obtain a very good fit to the low energy properties of the nucleon which is summarized in table 2. A similar calculation[7] for mesons

yields $m_\pi \simeq 177$ MeV, $m_\rho \simeq 735$ MeV and $f_\pi \simeq 147$ MeV. Thus, the model provides a very successful low energy phenomenology.

5.1 Calculation of structure functions

In this section,we seek to extend the success of Wilets et al. to the deep inelastic regime by applying the methods of ref. [1] to the soliton model. This has three advantages over our previous calculations in the MIT bag. First, the momentum projection techniques of ref. [5] allow an unambiguous determination of the mass of the system *including* center-of-mass corrections which has not been available in our previous work. Second, in this model the confining forces are represented by a dynamical field and therefore the valence quarks are not required to carry all the momentum. Finally, the model provides a description of the empty bag state and therefore we may calculate the empty bag-empty bag matrix elements that appear in the expressions for quark distributions.

We obtain the valence quark distribution shown in Fig. 7. For comparison, we have also shown the valence quark distribution for the MIT bag calculated in ref. [1]. The smaller area under the soliton curve is a result of the momentum carried by the σ degrees of freedom, which we find to be about 30%. The spreading of the curve is a result of the fact that the quark wavefunctions are not approximate eigenstates of $|\mathbf{p}|$, as in the MIT bag.

The valence distribution is evolved to $Q^2 = 15$ GeV^2 using next to leading order QCD perturbation [6] theory for $\mu_0^2 = 0.6, 0.7, 0.8$ GeV^2. The results are shown in Fig. 8, along with data for $xu_v - xd_v$ from the CDHS Collaboration [7]. The calculated curves track the data for $x \gtrsim 0.3$ and are too large in the smaller x region. In this region one expects the effect of virtual mesons in the nucleon wavefunction to become non-negligible. In particular, these mesons will create a nonperturbative sea, which will

cause the valence quarks to lose momentum and perhaps lower the curve at small x.

5.6 Discussion

We mention some problems with our approach that should be mentioned prior to our final assessment of the results shown in Figs. 7 and 8. First, we observe that the soliton bag structure functions have a tail of very small magnitude that extends beyond $x = 1$. (The support is almost, but not quite perfect.) We believe this is due to our use of a proton state that is not an exact eigenstate of the model hamiltonian. Our proton has small admixtures of excited states of mass higher than the proton, causing values of $x > 1$ to be allowed. A related question concerns the sum rule for the number of valence quarks. Our calculation respects this sum rule if one integrates over the entire region, $x \geq 0$. If one integrates from 0 to 1, there is a small error (about 1%) caused by the extended tail of the distribution. We expect both problems (at high x) to disappear as the ansatz for the nucleon wave function is improved. Thomas [20] has discussed another approach to deal with these support problems.

We conclude from fig. 8 that the momentum projected soliton bag model of ref. [5] provides us with a good description of both the high and low energy scattering properties of the nucleon, except at high x. The model of ref. [5] does not incorporate chiral symmetry and consequently cannot describe the low x region where meson exchange effects are expected to be important. Several authors [28] have considered soliton models that have chiral symmetry. Perhaps the combination of the ideas of ref. [5] and chiral symmetry will yield improved results for the valence distributions.

6. Summary

One might think of a number of technical problems. Many are mentioned in Refs. 9-12. The most important is the sensitivity of the results to the value of μ_0^2. Jaffe and Ross argued that $\mu_0^2 = 0.5$ GeV^2 was needed to describe the Q^2 dependence of ratios

of moments of structure functions. This conclusion should be reviewed. If found firm, calculations[20] much employing $\mu_0^2 = 0.1$ GeV^2 would not be capable of describing the Q^2 dependence of structure functions.

If one takes $\mu_0^2 \approx 0.5$ GeV^2, the firm conclusion is that the confinement mechanism must be dynamical. This is necessary to ensure that quarks do not carry the entire momentum of the nucleon.

We believe that models with dynamical confinement, e.g. Refs. 11 and 12, provided are sufficiently accurate to be applied to calculate deep inelastic scattering from the nucleus.

List of References

1. H. Abramowicz *et al.*, Z. Phys. C. **25**, 29 (1984).
2. F. E. Close, "An Introduction to Quarks and Partons", Academic Press London, 1979; F. Halzen and A.D. Martin, "Quarks and Leptons", John Wiley & Sons, New York, 1984.
3. T. DeGrand, R.L. Jaffe, K. Johnson, and J. Kiskis, Phys. Rev. D **12**, 2060 (1975).
4. A.W. Thomas, J. Phys. G **7**, 6283(1981); S. Théberge, A.W. Thomas, and G.A. Miller, Phys. Rev. D **22**, 2838 (1980); A. W. Thomas, Adv. Nucl. Phys. **13**, 1 (1984); G.A. Miller, in ***Quarks and Nuclei***, edited by W. Weise (World Scientific, *Singapore*, 1984), vol. 1, p. 189.
5. M.C. Birse, E.M. Henley, G. Lübeck and L. Wilets, in: Solitons in nuclear and elementary particle physics, Proc. 1984 Lewes Workshop, eds. A. Chodos, E. Hadjimichael and H.C. Tze (World Scientific, Singapore, 1984) p. 189; E.G. Lübeck, M.C. Birse, E.M. Henley and L. Wilets, Phys. Rev. D 33 (1986) 234.
6. R. Friedberg and T.D. Lee, Phys. Rev. D 15 (1977) 1694; D 16 (1977) 1096; D 18 (1978) 2623.
7. L. Wilets, "The Nontopological Soliton Model", World Scientific, 1989.
8. See eg the reviews U. Meissner, L. Vepstas, A.D. Jackson, Phys. Rep. 187, 109 (1990).
9. J.J. Aubert *et. al.*, Phys. Lett. **123B**, 275 (1983); A. Bodek *et al.*, Phys. Rev. Lett. **50**, 1431 (1983); **51**, 534 (1983); R.G. Arnold *et. al., ibid.* **52**, 727 (1984); A.C. Benvenuti *et al.*, in ***Proceedings of the 22nd International Conference on High Energy Physics***, Leipzig, 1984, edited by A. Meyer and E. Wieczorek (Akademie der Wissenschaften der DDR, Zeuthen, East Germany, 1984), Vol. 1, p. 219.

10. C.J. Benesh, University of Washington, Ph.D Thesis 1988.
11. C.J. Benesh and G.A. Miller, Phys. Rev. D **36**, 1344 (1987).
12. C.J. Benesh and G.A. Miller, Phys. Rev. D **38**, 48 (1988).
13. C.J. Benesh and G.A. Miller, Phys. Lett. **B215**, 381 (1988).
14. R.L. Jaffe, in ***Relativistic Dynamics and Quark Nuclear Physics***, proceedings of the Los Alamos School, 1985, edited by M.B. Johnson and A. Picklesimer (Wiley, New York, 1986).
15. R.L. Jaffe and G.G. Ross, Phys. Lett. **93B**, 313 (1980).
16. R.L. Jaffe, Phys. Rev. D **11**, 1953 (1975).
17. A.J. Buras, Rev. Mod. Phys. **52**, 199 (1980).
18. M. Pennington and G.G. Ross, Phys. Lett. **86B**, 371 (1979).
19. H. Abramowicz *et al.*, Z. Phys. C **17**, 283 (1983).
20. A.J. Signal and A.W. Thomas PRD 40, 2832 (1989)
    A.W. Thomas Nucl. Phys. **A532**, 177C (1991).
21. P.A.M. Dirac, Proc. R. Soc. London **A268**, 57 (1962).
22. P. Gnädig, P. Hasenfratz, J. Kuti, and A.S. Szalay, Phys. Lett. **64B**, 62 (1976); P. Hasenfratz and J. Kuti, Phys. Rep. **40**, 75 (1978).
23. K. Johnson, in ***Particles and Fields – 1979***, Annual Meeting of the Division of Particles and Fields of the APS, Montreal, Canada, 1979, edited by B. Margolis and D.G. Stairs (AIP Conf. Proc. No. 59) (AIP, New York, 1980), p. 353; erratum (unpublished).
24. A similar formalism was used by G.E. Brown, J. W. Durso, and M.B. Johnson, Nucl. Phys. **A397**, 447 (1983).

25. J.D. Sullivan, Phys. Rev. D5, 1732 (1972).

26. M. Ericson and A.W. Thomas, Phys. Lett. **128B**, 112 (1983);
R.P. Bickerstaff and G.A. Miller, *ibid.* **168B**, 409 (1986).

27. N.N. Nikolaev, Tokyo Report No. INS-Rep-539, 1985 (unpublished).

28. A.G. Williams and L.R. Dodd, Phys. Rev. D 37 (1988) 1971;
G. Fai, R.J. Perry and L. Wilets, Phys. Lett. B 208 (1988) 1.

Figure Captions

Figure 1. Deep inelastic scattering.

Figure 2. Deep inelastic scattering is related to the imaginary part of the forward Compton scattering amplitude.

Figure 3. Valence-quark distributions at the bag scale for projected and unprojected MIT bag.

Figure 4. Results of QCD evolution to $Q^2 = 15$ GeV^2. The solid curve is first-order evolution ($\mu_0^2 = 0.5$ GeV^2). The dashed curves are second-order evolution for $\mu_0^2 = 0.4$, 0.5, 0.6 GeV^2.

Figure 5. Valence-quark distribution for the nucleon at the bag scale, vibrating bag model.

Figure 6. Valence-quark distribution for the nucleon at $Q^2 = 15$ GeV^2, vibrating bag model.

Figure 7. Valence quark distributions at the bag scale for MIT and soliton bag.

Figure 8. Results of QCD evolution to $Q^2 = 15$ GeV^2.

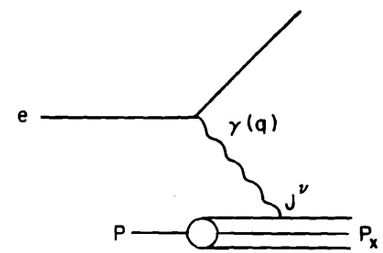

Figure 1

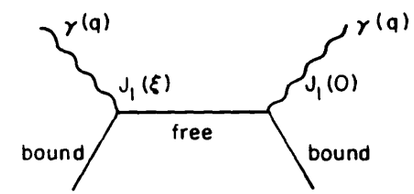

Figure 2

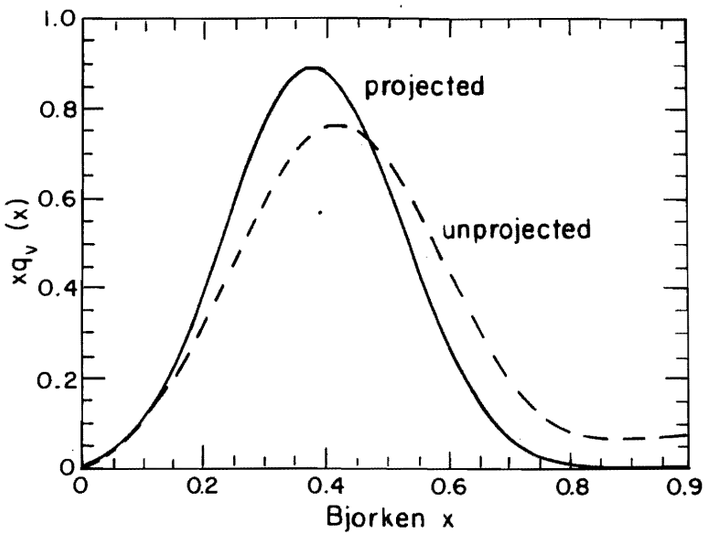

Figure 3

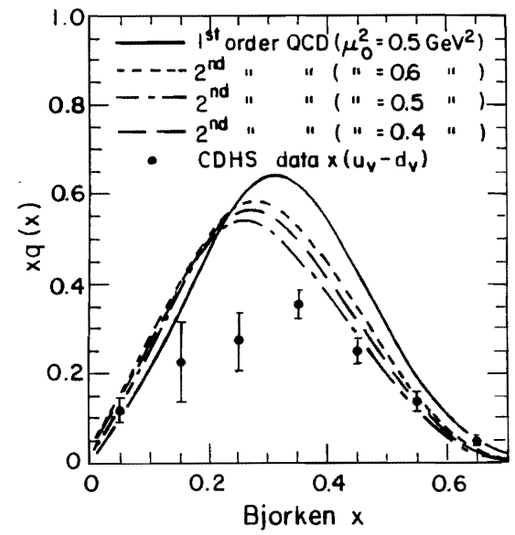

Figure 4

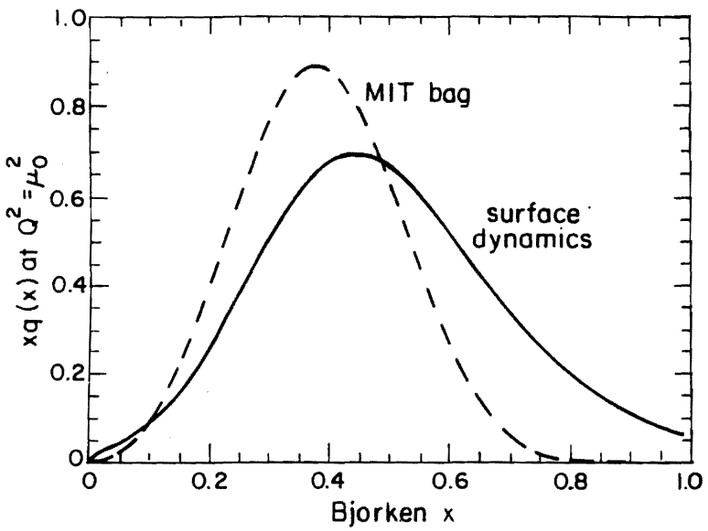

Figure 5

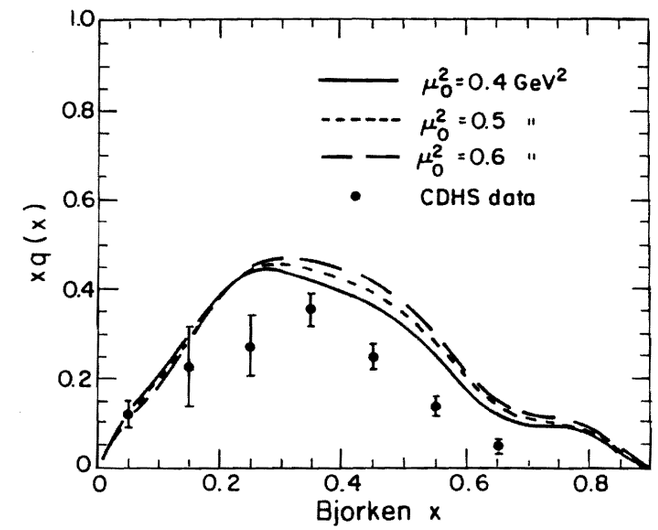

Figure 6

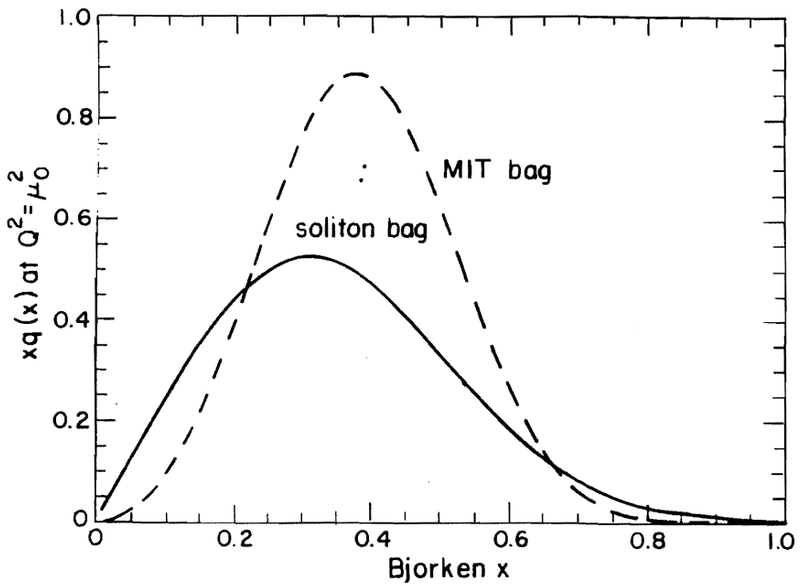

Figure 7

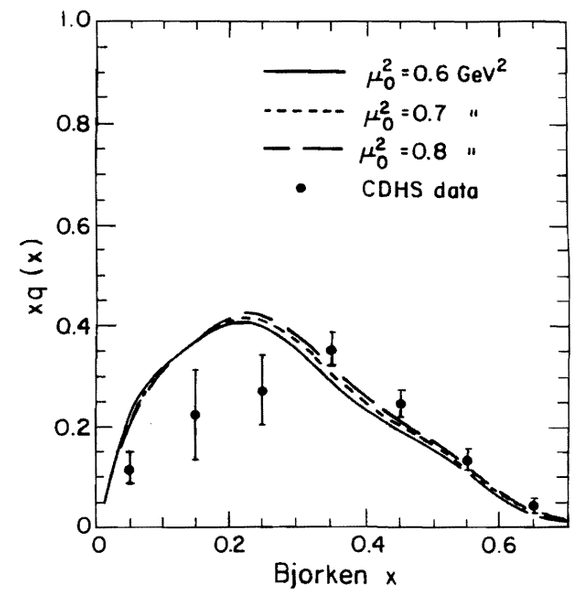

Figure 8